J. Fluid Mech. (1994), vol. 278, pp. 175–200
Copyright © 1994 Cambridge University Press

Stability analysis and large-eddy simulation of rotating turbulence with organized eddies

By CLAUDE CAMBON[1], JEAN-PIERRE BENOIT[1], LIANG SHAO[1] AND LAURENT JACQUIN[2]

[1] Ecole Centrale de Lyon / Université Claude Bernard, Lyon 1, Laboratoire de Mécanique des Fluides et d'Acoustique, URA CNRS no. 263, BP 163, 69131 Ecully Cedex, France

[2] Office National d'Etudes et de Recherches Aérospatiales, BP 72, 92320 Châtillon Cedex, France

(Received 16 August 1993 and in revised form 9 May 1994)

Rotation strongly affects the stability of turbulent flows in the presence of large eddies. In this paper, we examine the applicability of the classic Bradshaw–Richardson criterion to flows more general than a simple combination of rotation and pure shear. Two approaches are used. Firstly the linearized theory is applied to a class of rotating two-dimensional flows having arbitrary rates of strain and vorticity and streamfunctions that are quadratic. This class includes simple shear and elliptic flows as special cases. Secondly, we describe a large-eddy simulation of initially quasi-homogeneous three-dimensional turbulence superimposed on a periodic array of two-dimensional Taylor–Green vortices in a rotating frame.

The results of both approaches indicate that, for a large structure of vorticity W and subject to rotation Ω, maximum destabilization is obtained for zero *tilting vorticity* ($\frac{1}{2}W + 2\Omega = 0$) whereas stability occurs for zero absolute vorticity ($W + 2\Omega = 0$). These results are consistent with the Bradshaw–Richardson criterion; however the numerical results show that in other cases the Bradshaw–Richardson number

$$B = 2\Omega(W + 2\Omega)/W^2$$

is not always a good indicator of the flow stability.

1. Introduction

Rotating turbulent flows occur in fields as diverse as engineering (e.g. turbomachinery, reciprocating engines with swirl and tumble), geophysics and astrophysics. Studies of such flows have shown complex coupling between Coriolis forces, pressure and strain. Rotation is also an important factor in certain mechanisms of flows instability, such as the well-known elliptical flow instability, and strongly affects nonlinear interactions. Effects of curvature and advection by large eddies can often be considered as similar to those of rotation and analysed in the same way.

The aim of this paper is to study the combined effects of large-scale structures and rotation using simple modelling to elucidate the stability of such flows.

A number of recent studies in this area were presented at a Euromech colloquium, henceforth referred to as *E288* (see Cambon 1994). In particular, the behaviour of two-dimensional eddies imbedded in three-dimensional turbulence and subject to three-dimensional instabilities was described. The approaches reported included stability theory, direct numerical simulation and experimental measurements.

A striking conclusion of all approaches is that turbulent production is greater in regions of the flow where there is large-scale vorticity *and* strain than where there is strain alone. Futhermore, in regions of flow convergence, large dissipation and nonlinearity can become comparable to and even dominate turbulent production due to vortex stretching by the background flow. Three-dimensional secondary instabilities due to rotation, such as the elliptical flow instability, can eventually generate more turbulent energy than classical two-dimensional instabilities, such as the inflexional one (Kelvin–Helmholtz). For instance, the amplification factors of the most unstable modes are respectively $\exp(0.2St)$ for the K–H instability, with S the shear rate, and $\exp(\frac{9}{16}St)$ for the elliptical flow instability, with S the additional strain rate, as shown by Waleffe (1989); the explosive character of the latter instability is illustrated by the experiment of Malkus & Waleffe (1991).

The growth of three-dimensional disturbances is often linked to the loss of stability and subsequent breakdown of the large-scale structures. In particular, this was found to be the case for quasi-two-dimensional eddies in a rotating flow when the angular velocity of the eddies was of comparable magnitude and opposite in sense to that of the overall rotation (Bidokhti & Tritton 1992; Métais *et al.* 1991).

The discussions provoked by these results indicated an important difficulty concerning the distinction between the background flow, the large-scale structures and the turbulence. Some large eddies may appear as part of either the background flow or the disturbance to that flow, depending upon one's choice of statistical or large-scale filter. The linear or nonlinear character of certain interactions as well as the turbulent kinetic energy budget and the definition of crucial Rossby numbers (macro or micro, global or local) could also be dependent on the chosen split.

The aim of this paper is to attempt to resolve some of the above problems using simple idealized flows, rather than addressing more complex cases. We consider a flow in a rotating frame of reference and the main question addressed is the following: Given a large-scale structure of vorticity $\boldsymbol{W}$ containing fine-grained turbulence and a background angular velocity $\boldsymbol{\Omega}$, is it possible to characterize the stability of the structure by a single non-dimensional parameter, such as

$$R = \frac{4\Omega^2}{2\boldsymbol{\Omega}\cdot\boldsymbol{W}} = \frac{2\Omega}{W}, \tag{1.1}$$

the rotation number? Here, $\boldsymbol{W} = \nabla \times \boldsymbol{U}$ is the vorticity, which is *twice* the instantaneous angular velocity of a fluid particle, and the flow is observed in the rotating frame. The flow $\boldsymbol{U}$ is assumed to be quasi-two-dimensional in planes perpendicular to the rotation vector $\boldsymbol{\Omega}$. Thus $\boldsymbol{W}$ lies in the direction of $\boldsymbol{\Omega}$ and has component W in that direction. A simple, but incorrect criterion for maximum destabilization has been suggested by some authors (Lesieur 1990). This states that the angular velocity of the frame should balance the local angular velocity of the structure under consideration; symbolically

$$\boldsymbol{W} + 2\boldsymbol{\Omega} = 0 \quad (\text{ or } R = -1). \tag{1.2}$$

The suggested condition for maximum destabilization is easily seen to be incorrect: turbulence with zero absolute vorticity can be considered as subject to pure strain; however *the principal axes of strain are continuously rotating*, so that the time-averaged production of turbulent vorticity by vortex stretching is zero. This fact will be derived in § 2 using Cauchy's solution of the Helmholtz equation and is illustrated by the experiment of Gence & Mathieu (1979). In addition, the stability analysis of elliptical

flow in a rotating frame (Craik 1989), extensively rediscussed below, shows that the case of zero absolute vorticity is a unique case, that is unconditionally stable.

It will be shown in this paper that the criterion for maximum instability is one of zero *tilting vorticity*

$$\tfrac{1}{2}\boldsymbol{W} + 2\boldsymbol{\Omega} = 0 \quad (\text{or } R = -\tfrac{1}{2}). \tag{1.3}$$

The word *tilting* refers to the conventional distinction between *vortex stretching* and *vortex tilting* terms in the equation that governs the vorticity, and which are given in § 2. In the case of zero tilting vorticity, the background rotation balances only one half of the local angular velocity of the structure. This criterion is consistent with the results of Bradshaw (1969). This author studied the case of simple uniform shear in a rotating frame (for which the rotation number is $R = -2\Omega/S$ with shear rate S), and on the grounds of an analogy between rotation curvature and density stratification, proposed that flow stability is governed by the Bradshaw–Richardson number

$$B = R(R+1),$$

which involves the product of the background angular velocity Ω, and absolute vorticity $2\Omega - S$. According to Bradshaw, the flow is stable if $B > 0$ and, since the analysis is linearized, we find the forms

exponential growth as	$\exp\left[\lvert B\rvert^{1/2} St\right]$	for $B < 0$ (so-called unstable case),
linear growth as	St	for $B = 0$ (so-called neutral case),
oscillating behaviour as	$\exp\left[\mathrm{i}\lvert B\rvert^{1/2} St\right]$	for $B > 0$ (so-called stable case).

The maximum growth rate is found for $B = -\frac{1}{4}$ (or $R = -\frac{1}{2}$) in agreement with the criterion (1.3) of zero tilting vorticity. It is important to note that, in addition to being inviscid (which we shall see is not a great restriction), Bradshaw's analysis is limited in that it ultimately derives from a *displaced particle* approach, similar to Rayleigh's (1916) derivation of his classic stability criterion for flows under rotation. Indeed, Bradshaw's result is a special case of the Rayleigh criterion, as shown in Appendix A.

The use of *displaced particle* arguments amounts to neglecting the pressure perturbation terms within linear stability theory and is an approximation. This approximation was, in effect, also used by Tritton (1992) who found the Bradshaw stability criterion by an argument of flow impulse. The fact that these analyses are two-dimensional and pressure-less is a weakness, but a true three-dimensional stability analysis of Pedley (1969) for a rotating pipe could support them partly. Speziale, Gatski & Mac Giolla Mhuiris (1990) and Jacquin, Salhi & Benoit (1992) have considered classical approximate turbulent Reynolds-stress models that also do not lead to the exact equations in the linear limit. It is interesting to observe that, in that limit, their results indicate a (moderately) different stability criterion from that of Bradshaw.

Using what amounts to exact inviscid linear stability theory (but interpreted in terms of turbulent correlations in a rapid distortion theory – RDT – fashion), Bertoglio (1982) and Salhi (1992) have also found that the Bradshaw criterion is not fulfilled. However, they show that the criterion $R = -\frac{1}{2}$ for maximum destabilization is respected. Their results are in agreement with those of Bardina, Ferziger & Reynolds (1983) using large-eddy simulation (LES).

In the different context of mixing layers, the stability analysis of Yanase *et al.* (1992) and experimental results of Bidokhti & Tritton (1992) seem to confirm the criterion of zero tilting vorticity for maximum destabilization. Uncertainty remains, however, since the rotation numbers of these studies are obtained from an average shear across

the layer, and not from the local vorticity of the large structures. The same remarks hold for experimental (Johnston, Halleen & Lezius 1972) and numerical (Andersson & Kristoffersen 1992; Kristoffersen & Andersson 1993) works in rotating channel flows.

There appears then to be a reasonably convincing body of evidence that maximum destabilization is obtained for zero tilting vorticity and, as stated before, the case of zero absolute vorticity should lead to stability (Craik 1989).

Direct numerical simulation (DNS) of mixing layers and wakes was carried out by Métais *et al.* (1991), resulting in visualizations which were interpreted (Lesieur 1990) as showing that maximum destabilization occurs for zero absolute vorticity and that the Taylor–Proudman theorem gives the stability criterion for large enough rotation numbers. Although we believe this interpretation to be questionable, we consider that these results have provoked an interesting debate and, to a certain extent, have motivated the present study.

The instability of elliptical flows with rotation was considered by Craik (1989) and is particularly relevant to the present study. Among other results, he found stability for zero absolute vorticity ($W + 2\Omega = 0$). In all other cases, the flow was unstable to some initial perturbation, but the instability was found to be particularly striking when the tilting vorticity is zero. These instabilities were found to be relatively weak when the elliptic vortex rotates in the same sense as the background rotation ($R > 0$), a case we will later refer to as *cyclonic*, after the conventional use in the geophysical community. Some of the results of Bradshaw's 'pressure-less' stability analysis are thus reflected by *exact* linear stability theory of the rotating infinite elliptical eddy. Nonetheless, a single parameter, such as B, does not fully describe the stability problem, nor is Bradshaw's criterion fully justified.

In order to apply and extend these results to a large-scale structure in a rotating flow, exact stability analyses and large-eddy simulations have been undertaken and the results are described in this paper, which is organized as follows.

Section 2 reviews the basic equations and shows how one can relate equivalent formulations in terms of velocity and vorticity. The roles of absolute and tilting vorticity are brought to the fore.

In § 3 we consider the stability of flows with a quadratic streamfunction. These flows are characterized by constant gradients of velocity and can be the background flows for homogeneous turbulence, according to Craya (1958). Cambon (1982) and Cambon, Teissèdre & Jeandel (1985, hereafter referred to as CTJ) have studied the stability of such flows and have provided subsequent RDT solutions for a wide range of the parameter $2D/W$ (where D, the strain rate, and W, the vorticity, define the velocity gradient matrix). The range studied included those of hyperbolic streamlines (strain dominated, $2D/W > 1$), linear streamlines (simple shear, $2D/W = 1$) and elliptical streamlines (vorticity dominated, $2D/W < 1$). The latter class has more recently attracted a lot of interest and several studies appeared in 1986 (those of Pierrehumbert, Bayly, Craik & Criminale). These studies will collectively be referred to as PBCC. Recent reviews can be found in *E288* and Waleffe (1989, 1992).

The limitation of quadratic flows is that they are infinite in extent and therefore are not a very realistic model of a finite vortical structure. We would like to consider flows which include rotational regions and also strain-dominated (or convergence) zones.

In § 4, a more realistic, but still idealized model flow is examined. The flow initially consists of a periodic lattice of two-dimensional Taylor–Green vortices in a rotating frame of reference with three-dimensional fine-scale turbulence superimposed. Half

of the vortices are cyclonic and half are anticyclonic. The evolution of the flow is calculated by large-eddy simulation. Note that the large-scale strain rate D and vorticity W vary throughout the flow. These parameters are constant for the quadratic flows of § 3, but now the ratio $2D/W$ can vary from zero at the core of the eddy to infinity between eddies. A similar flow configuration was studied, both experimentally and numerically, by Michard *et al.* (1986) in the absence of background rotation.

Finally, in § 5, the effects of rotation on initially unstructured turbulence are briefly reviewed in the light of our results.

2. Reviewing the basic equations

The Euler and Helmholtz equations for an incompressible velocity field are written for velocity, pressure and vorticity ($\boldsymbol{U}, P, \boldsymbol{W} = \nabla \times \boldsymbol{U}$), in a rotating frame. The equation for the total (mean plus fluctuation) absolute vorticity in the Galilean reference frame and its formal solution (found over a hundred years ago by Cauchy, Kelvin and Weber) is not very helpful, since the implicit effect of system rotation on the total strain $\frac{1}{2}(U_{i,j} + U_{j,i})$ is not known. Hence, *linearized* equations in the *rotating* frame are discussed below. For convenience, each quantity is split into a background (mean) part and a perturbation (fluctuation) part, so that henceforth

$$\boldsymbol{U} \rightarrow \boldsymbol{U} + \boldsymbol{u}; \quad P \rightarrow P + p; \quad \boldsymbol{W} \rightarrow \boldsymbol{W} + \boldsymbol{\omega}.$$

The linearized vorticity equation reads

$$\dot{\omega}_i + u_j W_{i,j} = U_{i,j}\,\omega_j + u_{i,j}\,(W_j + 2\,\Omega_j), \tag{2.1}$$

where the superscript dot $(\dot{\ })$ in the first term on the left-hand side denotes the advective terms

$$(\dot{\ }) = (\ )_{,t} + U_j(\ )_{,j}.$$

The second term on the left-hand side is essential for inflexional instability (see Appendix B) but is not important for three-dimensional instabilities modified by rotation; hence it will be neglected at this stage, so that

$$W_{i,j} \sim 0, \tag{2.2}$$

to be taken into account later in § 4.

The two terms on the right-hand side of (2.1) are the result of linearizing the basic *vortex stretching* term $U_{i,j}(W_j + 2\Omega_j)$. Assuming that the absolute vorticity has zero value, (2.1) has a simple Cauchy's solution

$$\omega_i(\boldsymbol{x}, t) = F_{ij}(\boldsymbol{X}, t, 0)\,\omega_j(\boldsymbol{X}, 0), \tag{2.3}$$

where $\boldsymbol{X}$ is the position at time $t = 0$ (the third argument of F_{ij} in (2.3)) of a particle of the mean flow, which reaches the Eulerian position $\boldsymbol{x}$ at time t; $F_{ij} = \partial x_i/\partial X_j$ is the conventional displacement gradient (Eringen 1967) defined by

$$\mathrm{d}x_i = U_i\,\mathrm{d}t + F_{ij}\,\mathrm{d}X_j. \tag{2.4}$$

Following another conventional formalism, (2.1) has a slighty different form:

$$\dot{\omega}_i = U_{i,j}\,\omega_j - \epsilon_{ijl}\,(W_j + 2\Omega_j)\,\omega_l + u_{j,i}\,(W_j + 2\Omega_j)$$

or (using a more popular vector notation)

$$\frac{\mathrm{D}\boldsymbol{\omega}}{\mathrm{D}t} = \boldsymbol{\omega} \cdot \nabla \boldsymbol{U} - (\boldsymbol{W} + 2\boldsymbol{\Omega}) \times \boldsymbol{\omega} + \nabla[\boldsymbol{u} \cdot (\boldsymbol{W} + 2\boldsymbol{\Omega})] \tag{2.5a}$$

in accordance with (2.2) and $u_{i,j} = u_{j,i} + \epsilon_{ilj}\omega_l$. The corresponding linearized equation for $\boldsymbol{u}$ reads

$$\dot{u}_i = -U_{i,j}u_j - 2\epsilon_{ilj}\Omega_l u_j - p_{,i}. \tag{2.5b}$$

In order to reconcile the vorticity and velocity approaches and to derive a unique form of these equations, the background velocity gradient is split into symmetric (strain) and antisymmetric parts:

$$\left.\begin{aligned} U_{i,j} &= S_{ij} + W_{ij}, \\ S_{ij} &= \tfrac{1}{2}(U_{i,j} + U_{j,i}), \\ W_{ij} &= \tfrac{1}{2}(U_{i,j} - U_{j,i}) = \tfrac{1}{2}\epsilon_{ilj}W_l. \end{aligned}\right\} \tag{2.6}$$

Accordingly, (2.5*a*) and (2.5*b*) become

$$\dot{\boldsymbol{\omega}} = \boldsymbol{S}\cdot\boldsymbol{\omega} - (\tfrac{1}{2}\boldsymbol{W} + 2\boldsymbol{\Omega}) \times \boldsymbol{\omega} + \nabla\,[\boldsymbol{u}\cdot(\boldsymbol{W} + 2\boldsymbol{\Omega})]\,, \tag{2.7a}$$

$$\dot{\boldsymbol{u}} = -\boldsymbol{S}\cdot\boldsymbol{u} - (\tfrac{1}{2}\boldsymbol{W} + 2\boldsymbol{\Omega}) \times \boldsymbol{u} - \nabla p, \tag{2.7b}$$

where the 'tilting vorticity' term $\frac{1}{2}\boldsymbol{W} + 2\boldsymbol{\Omega}$ is now displayed in both equations†. These equations (2.7*a*, *b*) can be closed by solving two similar Poisson equations

$$\nabla^2\boldsymbol{u} = -\nabla \times \boldsymbol{\omega}, \tag{2.8a}$$

$$\nabla^2 p = -2S_{ij}s_{ij} + (W_i + 2\Omega_i)\omega_i, \tag{2.8b}$$

with $s_{ij} = \frac{1}{2}(u_{i,j} + u_{j,i})$ as in (2.6).

In short, splitting the velocity gradient matrix into symmetric and skew-symetric parts exhibits the tilting vorticity as an explicit parameter for production of both enstrophy and energy. The absolute vorticity, however, is involved in Poisson equations associated with specific gradients terms.

Returning to the case of pure shear flow, we see that for the zero-absolute-vorticity criterion $R = -2\Omega/S = -1$, (2.3) leads to *linear* (in St) amplification terms. On the other hand, the solution of

$$\dot{\boldsymbol{\omega}} = \boldsymbol{S}\cdot\boldsymbol{\omega}$$

obtained for $R = -\frac{1}{2}$ (the Bradshaw criterion) when the pure gradient term is neglected in (2.7*a*), leads to *exponential* ($\exp[St/2]$) amplification coefficients for the case of pure shear, where S stands for the shear rate. These results are easily extended to more general fields; the effects of 'production-redistribution' that correspond to explicit terms in (2.7*a* or 2.7*b*) (and in the equations that govern $\langle u_i u_j\rangle$ or $\langle\omega_i\omega_j\rangle$) would induce maximum amplification when the tilting vorticity is zero.

Accordingly, it is possible to rewrite the equations so as to lend support to a generalized 'pressure-less' Bradshaw criterion, but the above analysis is not conclusive since the gradient terms in (2.7*a*, *b*) preclude finding an exact solution; a numerical procedure (which is described in § 3) is required.

† In fact, (2.7*a*) is not exactly recovered when taking the Curl of (2.7*b*), because (2.7*a*) takes into account the criterion (2.2) whereas no such additional assumption is used in (2.7*b*)

3. Linear stability analysis of quadratic flows and RDT computations

The purpose of this section is to obtain accurate solutions to the system (2.7) and (2.8) for disturbances to the simple basic flows initially considered by Craya (1958) and Lagnado, Phan-Thien & Leal (1984).

A plane *quadratic* basic flow can be defined using the following streamfunction in the plane (x_1,x_2):

$$\Psi = -\frac{D}{2}(x_1^2 - x_2^2) + \frac{W}{4}(x_1^2 + x_2^2) \; ; \quad U_1 = +\frac{\partial \Psi}{\partial x_2} \; ; \quad U_2 = -\frac{\partial \Psi}{\partial x_1}, \tag{3.1}$$

where D is the strain rate (or maximum stretching rate) and W the spanwise vorticity (or twice the local angular velocity). These flows can be seen to be a superimposition of a pure plane strain (D) and a solid-body rotation ($W/2$), having the constant velocity gradients

$$U_{i,j} = \begin{pmatrix} 0 & D - \frac{1}{2}W \\ D + \frac{1}{2}W & 0 \end{pmatrix} \quad \text{or} \quad U_{i,j} = \begin{pmatrix} D & -\frac{1}{2}W \\ +\frac{1}{2}W & -D \end{pmatrix}. \tag{3.2}$$

The latter expression is written in the principal axes of the associated pure strain, obtained after rotating an angle $\pi/4$ from the initial frame (x_1, x_2). Without lack of generality, D and W are chosen positive ($W < 0$ will be considered only in § 3.2 in order to recover the conventional case of pure shear: $D = -W/2$). The streamlines of the three cases are shown in figure 1. Stability analyses of these flows were done by CTJ and PBCC (for $W/2 > D$). Some analytic solutions were also given in particular cases by Lagnado *et al.* (1984). Complete numerical solutions, including the tabulation of the linear transfer matrix that generates the kernel, were used by CTJ to compute statistical correlations of the fluctuating field, such as is done in rapid distortion theory for homogeneous turbulence (Batchelor & Proudman 1954; Townsend 1956). Note that no reference was given by PBCC to any statistical application, since they consider a single Fourier component of the disturbance field, so that nonlinear interactions are zero, and their solutions can be seen as *exact*. In other words, the assumption of *weak* disturbance which allows linearization of the equations for the total field ($U_i \rightarrow U_i + u_i$) is not necessary if a single mode of $\hat{u}$ (defined below) is considered. Nevertheless, the starting point is the same as in RDT and the different approaches can be reconciled (see *E288* for more details on the underlying principles).

Within the rotating frame ($\Omega_i = \Omega\delta_{i3}$), the general method by CTJ is applied to solve the linearized problem with application to homogeneous solenoidal RDT. The fluctuating fields are expanded in terms of time-dependent Fourier modes $\exp[i\boldsymbol{k}(t)\cdot\boldsymbol{x}]$, where $\boldsymbol{k}$ is given by

$$\left.\begin{aligned} &\dot{k}_i = -U_{j,i}k_j; \quad k_i = F_{ji}^{-1}(t,0)K_j, \\ &\text{and} \qquad F_{ij} \begin{cases} F_{\alpha\beta} = \delta_{\alpha\beta}\cosh\sigma t + U_{\alpha,\beta}\dfrac{\sinh\sigma t}{\sigma} \\ F_{i3} = F_{3i} = \delta_{i3}, \end{cases} \\ &\text{with} \qquad \alpha,\beta = 1,2, \quad \sigma^2 = D^2 - \left(\tfrac{1}{2}W\right)^2, \end{aligned}\right\} \tag{3.3}$$

is the displacement gradient, as in (2.3) and (2.4). Capital and lower-case letters correspond respectively to Lagrangian (moving with the background field) and Eulerian

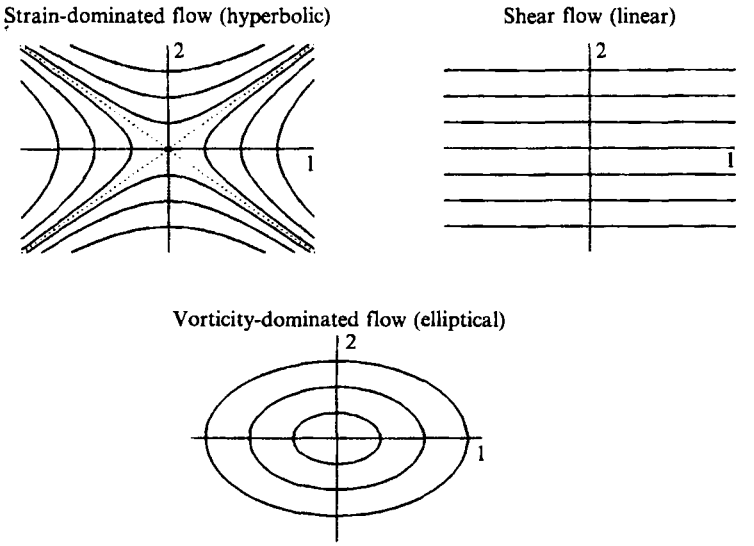

FIGURE 1. Streamlines of the background flows.

variables, in accordance with (2.4) and a wave conservation law

$$\boldsymbol{k} \cdot \boldsymbol{x} = \boldsymbol{K} \cdot \boldsymbol{X}.$$

The sign of $\sigma^2 = -\frac{1}{2}\nabla^2 P$ characterizes the class of the flow (where σ is either a real or a pure imaginary number), and provides a convenient link between some previous works (Craya 1958) and modern topological approaches (Chong, Perry & Cantwell 1990). Note that the *exact* single mode of the disturbance field

$$\hat{\boldsymbol{u}}(\boldsymbol{k}, t) \exp[\mathrm{i}\boldsymbol{k}(t)\cdot\boldsymbol{x}]$$

is more complex, in general, than the classic wave-like disturbance

$$\boldsymbol{A}(\boldsymbol{k}) \exp[\mathrm{i}(\boldsymbol{k}\cdot\boldsymbol{x} - C(\boldsymbol{k})\, t)]$$

used in conventional hydrodynamic stability analysis (see Appendix B). The hat ($\hat{}$) denotes a three-dimensional Fourier transform. The solution is not sought using the three-component Fourier transform $\hat{u}_i(\boldsymbol{k}, t)$, but instead the two solenoidal components $\hat{\varphi}_1$ and $\hat{\varphi}_2$, obtained by projecting $\hat{\boldsymbol{u}}$ on an orthonormal frame ($\boldsymbol{e}^1, \boldsymbol{e}^2, \boldsymbol{e}^3 = \boldsymbol{k}/k$) via the so-called Craya decomposition (see also Herring 1974):

$$\hat{\boldsymbol{u}}(\boldsymbol{k}, t) = \hat{\varphi}_1(\boldsymbol{k}, t)\boldsymbol{e}^1(\boldsymbol{k}) + \hat{\varphi}_2(\boldsymbol{k}, t)\boldsymbol{e}^2(\boldsymbol{k}), \tag{3.4a}$$

$$\hat{\boldsymbol{\omega}}(\boldsymbol{k}, t) = \mathrm{i}k\left(\hat{\varphi}_1(\boldsymbol{k}, t)\boldsymbol{e}^2(\boldsymbol{k}) - \hat{\varphi}_2(\boldsymbol{k}, t)\boldsymbol{e}^1(\boldsymbol{k})\right). \tag{3.4b}$$

Thus the incompressibility constraint ($\boldsymbol{k} \cdot \hat{\boldsymbol{u}} = 0$) is satisfied, the pressure effects are implicitely accounted for, and the initial problem in four components ($\hat{u}_1, \hat{u}_2, \hat{u}_3, \hat{p}$) reduces to one in two components. The use of two solenoidal mode intensities ($\hat{\varphi}_1$ and $\hat{\varphi}_2$) as dependent variables is more convenient than the use of two planar coordinates ($\hat{u}_1$ and $\hat{u}_2$, after elimination of $\hat{u}_3 = -(k_1\hat{u}_1 + k_2\hat{u}_2)/k_3$ and $\hat{p}$), as used by PBCC. Analytical solutions are often simpler in the frame ($\boldsymbol{e}^1, \boldsymbol{e}^2$) and furthermore the numerical computation is facilitated, because the actual linear solutions are expressed in coordinates that are more closely related to the eigenmodes. For instance, in the case of pure rotation, the *helical mode* intensities ($\hat{\varphi}_2 - \mathrm{i}\hat{\varphi}_1$, $\hat{\varphi}_2 + \mathrm{i}\hat{\varphi}_1$, $\mathrm{i}^2 = -1$) are

immediately recovered: they are the eigenmodes of the linear regime of inertial waves (Greenspan 1968; Cambon & Jacquin 1989; Waleffe 1992).

Choosing the *local* (angular-dependent wavevector) frame $(\boldsymbol{e}^1, \boldsymbol{e}^2)$ so that $\boldsymbol{e}^1$ is normal to $\boldsymbol{\Omega}$, (or $\boldsymbol{e}^1 = (\boldsymbol{k} \times \boldsymbol{n})/|\boldsymbol{k} \times \boldsymbol{n}|$ with $n_i = \delta_{i3}$), $\widehat{\varphi}_1$ and $\widehat{\varphi}_2$ are closely connected to the set $(\omega_3, \nabla^2 u_3)$ conventionally used for studying the stability of sheared flows in physical space (see Appendix B). It can easily be shown that

$$\widehat{\omega}_3 = -\mathrm{i}\,(k_1^2 + k_2^2)^{1/2}\,\widehat{\varphi}_1, \tag{3.5a}$$

$$\widehat{\nabla^2 u_3} = k\,(k_1^2 + k_2^2)^{1/2}\,\widehat{\varphi}_2 \tag{3.5b}$$

with $k = (k_i k_i)^{1/2}$.

The linear equation (2.5*b*) is three-dimensional Fourier transformed and used in the local frame $(\boldsymbol{e}^1, \boldsymbol{e}^2)$, so that

$$\dot{\widehat{\varphi}}_\alpha(\boldsymbol{k}, t) + m_{\alpha\beta}(\boldsymbol{k})\widehat{\varphi}_\beta(\boldsymbol{k}, t) = 0, \tag{3.6}$$

with $m_{\alpha\beta} = e_i^\alpha U_{i,j} e_j^\beta - \dot{e}_i^\alpha e_i^\beta + 2\Omega_l\,\epsilon_{ilj}\,e_i^\alpha e_j^\beta$. The Greek indices take only values 1 or 2, and the superscript dot $(\dot{})$ indicates a substantial time-derivative (as it does in physical space) at fixed $\boldsymbol{K}$, as in (3.3). Because of the orthonormal properties $(e_i^\alpha e_j^\alpha = \delta_{ij},\ e_i^\alpha e_i^\beta = \delta_{\alpha\beta})$ it is found that

$$\dot{e}_i^\alpha e_i^\beta = \epsilon_{\alpha\beta 3}\dot{e}_i^2 e_i^1 = -\epsilon_{\alpha\beta 3}\,e_i^2\,U_{i,j}\,e_j^1$$

so that the matrix

$$m_{\alpha\beta} = S_{ij}(e_i^\alpha e_j^\beta - \epsilon_{\alpha\beta 3}\,e_i^2 e_j^1) + \epsilon_{\alpha\beta 3}\,(W_l + 2\Omega_l)\frac{k_l}{k}$$

exhibits the projection of the absolute vorticity onto the wavevector, as the unique contribution from rotational terms:

$$m_{\alpha\beta} = \begin{pmatrix} 2aD & -\dfrac{k_3}{k}(W + 2\Omega) \\ 2cD + \dfrac{k_3}{k}(W + 2\Omega) & 2bD \end{pmatrix} \tag{3.7}$$

where the strain-related angular-dependent coefficients are $a = e_1^1 e_2^1$, $b = e_1^2 e_2^2$ and $c = e_1^2 e_2^1 + e_2^2 e_1^1$. For more details, the reader is referred to CTJ and Benoit (1992) or, if not acquainted with the French language, to Cambon, Coleman & Mansour (1993).

For zero absolute vorticity, equation (3.6) for $\widehat{\varphi}_1$ leads to $\dot{\widehat{\omega}}_3 = 0$, in agreement with (3.5) and, more generally, with the Cauchy solution in (2.3). Another interesting result is found for spanwise wavevectors (or $k_1 = k_2 = 0$). In this case, the local frame $(\boldsymbol{e}^1, \boldsymbol{e}^2)$ is not defined, and the fixed (planar) frame of reference is more convenient (as used also by Craik 1989) since $\widehat{u}_3 = 0$; accordingly $(\widehat{u}_1, \widehat{u}_2)$ are substituted into $(\widehat{\varphi}_1, \widehat{\varphi}_2)$, and the rank-two matrix $\boldsymbol{m}$ reduces to

$$\begin{pmatrix} D & -(\frac{1}{2}W + 2\Omega) \\ (\frac{1}{2}W + 2\Omega) & -D \end{pmatrix}, \tag{3.8}$$

recovering the tilting vorticity, consistent with the absence of pressure effects for these spanwise wavevectors.

The solution of (3.6) is characterized by a rank-two matrix $g_{\alpha\beta}$, which has to be tabulated for each wavevector inclination,

$$\widehat{\varphi}_\alpha(\boldsymbol{k},t) = g_{\alpha\beta}(\boldsymbol{k},t,0)\widehat{\varphi}_\beta(\boldsymbol{K},0). \tag{3.9}$$

Solving (3.6) in the general case is intricate because $\boldsymbol{k}$ is time-dependent, as shown by (3.3). Hence, a numerical code is used to derive the matrix $\boldsymbol{g}$ generating the solution of (3.6) and the first equation of (3.3), using a fourth-order Runge–Kutta method. The solutions for the covariance matrices such as $\langle \widehat{u}_i^* \widehat{u}_j \rangle$ or $\langle \widehat{\omega}_i^* \widehat{\omega}_j \rangle$ are then derived, choosing particular initial data. Here an initial isotropy is assumed,

$$\langle \widehat{u}_i^*(\boldsymbol{p},0)\widehat{u}_j(\boldsymbol{k},0)\rangle = \frac{E(k)}{4\pi k^2}\left(\delta_{ij} - \frac{k_i k_j}{k^2}\right)\delta(\boldsymbol{k}-\boldsymbol{p}),$$

and the covariance matrices are integrated over the $\boldsymbol{k}$-space in order to provide one-point velocity correlations, in agreement with conventional RDT (see Benoit 1992, for details on the numerical method). We note that the solutions for statistical correlations only involve the evolution of the matrix $\boldsymbol{g}$, which also gives the general solution of the linear stability problem (3.6). This matrix is close to the matrix denoted $\boldsymbol{A}$ by Townsend (1956) and to the Floquet matrix calculated by PBCC in the case of the *elliptical flow instability*.

Curves for *global* quantities (such as the kinetic energy $\frac{1}{2}q^2 = \frac{1}{2}\langle u_i u_i\rangle$ or enstrophy $\frac{1}{2}\langle \omega_i \omega_i\rangle$) will be presented below. On the one hand, these curves can be interpreted as histories of one-point correlations, in the field of homogeneous solenoidal RDT applied to *pre-existing isotropic turbulence*. On the other hand, they can be solely considered as a norm (average over all wavevector directions) of the matrix $\boldsymbol{g}$ (with no statistical interpretation) since the same weight is given to each initial wavevector independently of its angular position. This can be seen from the fact that

$$\frac{q^2}{q_0^2} = \frac{1}{2}\iint_{|\boldsymbol{K}|=1} g_{\alpha\beta}(\boldsymbol{k}(t),t,0)g_{\alpha\beta}(\boldsymbol{k}(t),t,0)\,\frac{\mathrm{d}\sigma_k}{4\pi},$$

$$\frac{\omega^2}{\omega_0^2} = \frac{1}{2}\iint_{|\boldsymbol{K}|=1} k^2(t)g_{\alpha\beta}(\boldsymbol{k}(t),t,0)g_{\alpha\beta}(\boldsymbol{k}(t),t,0)\,\frac{\mathrm{d}\sigma_k}{4\pi}.$$

3.1. *Hyperbolic (strain-dominated) flows*

For $D > W/2$, the streamfunction is hyperbolic and $\boldsymbol{F}$ (see (3.3)) involves real exponential terms, with

$$\sigma = \left(D^2 - \left(\tfrac{1}{2}W\right)^2\right)^{1/2}.$$

This case is considered here for the sake of completeness. The strong amplification shown in figure 2(*a*, *b*) for $2D/W = 1.2$ and several rotation numbers $2\Omega/W$ is probably not realistic, since nonlinearities and dissipation are very important in *actual* convergence zones (as stressed in *E288*). Nevertheless the *relative* position of the curves for different rotation numbers $2\Omega/W$ is believed to be physically correct.

The results shown in figure 2 confirm that the maximum destabilization is found for $R = -\frac{1}{2}$. Amplification of kinetic energy is reduced for $R = -1$ with respect to the case without rotation. The case $R = -1$, however, can be considered as destabilizing with respect to a *cyclonic* case ($R = 1$). Nevertheless, all the cases are destabilizing when looking at the enstrophy amplification, as figure 2(*b*) shows.

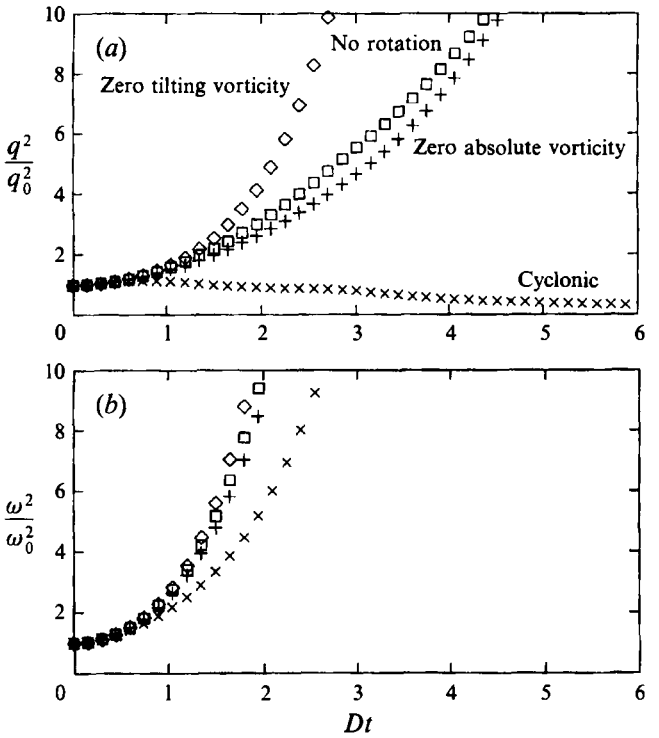

FIGURE 2. Kinetic energy (*a*) and enstrophy (*b*) histories for strain-dominated inviscid case: ◇, $R = -\frac{1}{2}$; □, $R = 0$; +, $R = -1$; ×, $R = 1$.

3.2. *Linear (pure shear) flows*

For $D = -W/2 = S/2$ $(W < 0)$, the pure shear flow of rate S is recovered so that

$$\sigma = 0 \qquad \text{and} \qquad F_{ij} = \delta_{ij} + U_{i,j}\, t$$

are consistent limits of (3.3) in this case. The relative position of the kinetic energy history curves in figure 3 (*a*) is the same as in the previous case.

Our numerical results for kinetic energy are in complete agreement with those of Bertoglio (1982) who solved the linear contribution to the equation for the velocity covariance matrix (the so-called Craya equation for double correlations); the link to the 'true' stability analysis, however, is lost in such an *a priori* statistical approach.

The difference between the $R = -\frac{1}{2}$ and $R = -1$ cases is particularly important. It can be seen that both cases $R = 0$ (without rotation) and $R = -1$ (zero absolute vorticity) correspond to the so-called *neutral* case ($B = 0$) if the Bradshaw–Richardson criterion is used.

Amplification of kinetic energy is shown in figure 3 (*a*) for both cases, but this result is very dependent on the presence of viscous effects, as the figure 3 (*b*) histories illustrate. Viscous effects can be introduced in the present stability analysis, as shown by CTJ and Landman & Saffman (1987).

In the particular case of pure shear, Lee, Kim & Moin (1990) have demonstrated that homogeneous RDT is applicable (they find near-wall turbulence structures at higher values of St) if viscous effects are accounted for. A first insight into the near-wall 'streaklike' structures can be obtained in pure inviscid homogeneous RDT when

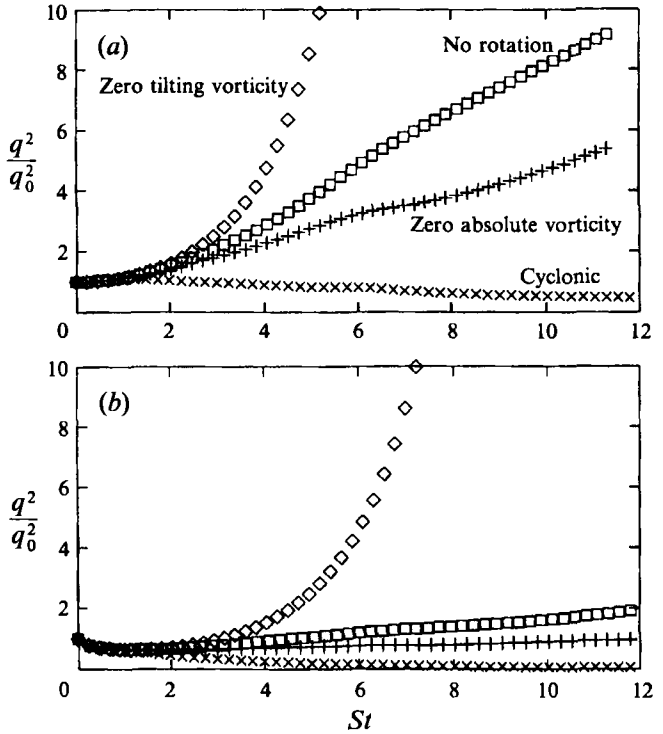

FIGURE 3. Kinetic energy histories for pure shear inviscid case (*a*), viscous case (*b*): ◇, $R = -\frac{1}{2}$; □, $R = 0$; +, $R = -1$; ×, $R = 1$.

looking at the history of some 'two-dimensional energy components' ($u_1^2 L_{11,1} \propto (St)^2$ and $u_1^2 L_{11,3} = constant$, see Cambon 1990) where $L_{11,1}$ is the streamwise integral length scale (related to the length of the streaklike structures) and $L_{11,3}$ the spanwise one (related to the spacing of the streaklike structures). Nevertheless, only *viscous* RDT can predict the relative values of the vorticity components, and in particular the eventual dominance of ω_1^2 over ω_3^2. In addition the very definition of a spacing scale $(\nu/S)^{1/2}$ is impossible without introducing the kinematic viscosity ν. Of course the accurate value of the actual streak spacing cannot be captured by linearized theories (Waleffe 1990), but qualitative trends can.

Hence, the results of figure 3(*b*) may be physically relevant to a more general flow pattern (representing a local region of high shear rate in an actual flow). This case deserves more attention and will be studied further in a subsequent paper. For analytical study, the simplest form of the equations is obtained choosing $\boldsymbol{n}$ as the vertical direction (in the definition of $\boldsymbol{e}^1, \boldsymbol{e}^2$), so that $\widehat{\varphi}_1$ and $k\widehat{\varphi}_2$ are linked to ω_2 and $\nabla^2 u_2$, respectively (see Appendix B).

3.3. *Elliptical (vorticity-dominated) flows*

For $D < W/2$, the elliptic eddy is recovered. Its periodic motion is characterized by the angular velocity $\Omega_0 = \left((W/2)^2 - D^2\right)^{1/2}$, in accordance with $\sigma =$

$\mathrm{i}\left((W/2)^2 - D^2\right)^{1/2} = \mathrm{i}\Omega_0$ in (3.3). The aspect ratio of the eddy is

$$E = \left(\frac{\frac{1}{2}W + D}{\frac{1}{2}W - D}\right)^{1/2}.$$

Instability mechanisms in the presence of this flow are of particular interest. This instability is often called *broad-band* (PBCC) when considering the wavevector modulus of the disturbance. It is obvious that no lengthscale information is given in the linear problem without boundary effects. This is reflected by the fact that the Floquet matrix $\boldsymbol{g}$ depends only on the *orientation* of the wavevector (or $\cos\theta = k_3/k$).

Hence, the disturbance associated with the elliptical flow is characterized by a *narrow-band* instability domain with respect to $\cos\theta$. This parametric instability develops with exponential growth, although the basic matrices ($\boldsymbol{F}$, $\boldsymbol{m}$) of the linear problem are time-periodic. The case of elliptical flow seems to be of prime importance regarding its implications for turbulence theory and modelling, as shown in the most recent studies of Waleffe (1989,1993). These studies include (in addition to the earlier works of Cambon 1982; CTJ; PBCC) applications to the elliptical eddy of finite size (height and diameter) and nonlinear analysis of the interactions between the background field and the two main unstable modes. Ideas for explaining a possible breakdown of the background field and the collapse of fundamental wavy disturbances were proposed, as was an elegant interpretation of the fundamental triadic interaction in turbulent flows. Some of these ideas were illustrated by the Malkus experiment (see Waleffe 1989; Malkus & Waleffe 1991): the elliptical flow is created inside a rotating cylinder (with the angular velocity Ω_0) and subjected to an additional weak strain by fixed rollers. With respect to the Malkus approach, the experimental and theoretical study by Benoit (1992), previously quoted, dealt with the case of pre-existing developed turbulence in the presence of the elliptical (or hyperbolic, or linear) flow (see also Leuchter, Benoit & Cambon 1992).

Much of what follows in this subsection is to be found in the analysis of Craik (1989), but using the different notation and numerical method of the present paper.

For the elliptical flow within a rotating frame, (3.3) is not modified (by the rotation of the frame), whereas the absolute vorticity ($2\Omega + W$) replaces W in the matrix $\boldsymbol{m}$ in (3.7), except for spanwise wavevectors ($k_1 = k_2 = 0$) where the tilting vorticity ($2\Omega + \frac{1}{2}W$) is displayed. At vanishing D, the disturbances consist of helical modes of opposite polarity ($\widehat{\varphi}_2 - \mathrm{i}\varepsilon\widehat{\varphi}_1$, $\varepsilon = \pm 1$) having the phase

$$\boldsymbol{k}\cdot\boldsymbol{x} + \varepsilon(2\Omega + W)\cos\theta \quad ; \quad \cos\theta = k_3/k$$

in agreement with the mathematical description of inertial waves (Greenspan 1968).

Following an argument successfully used by Bayly (1986), Waleffe (1989) and Craik (1989), the instability develops if the period of the wavevector motion coincides with the period of inertial waves, such as

$$|2\Omega + W|\cos\theta = \left(\left(\tfrac{1}{2}W\right)^2 - D^2\right)^{1/2}, \tag{3.10}$$

where $\cos\theta$ is chosen positive without loss of generality.

Without rotation of the frame, the unstable oblique modes around $\cos\theta = \frac{1}{2}$ are recovered, which is given by (3.10) at vanishing D. For this case, the rotation creates a shift of the instability peak (in $\cos\theta$) and kills off the instability for zero absolute vorticity. Three situations can be discussed:

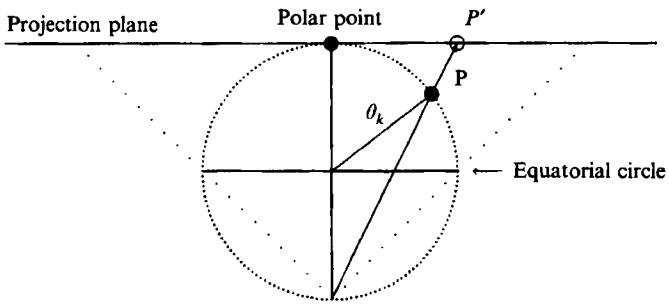

FIGURE 5. Geometry of the polar stereographic projection.

(i) Zero absolute vorticity. Analytical time-periodic solutions for $\boldsymbol{g}$ correspond to a pure strain whose principal axes are continuously rotated. The matrix $\boldsymbol{g}$ is periodic so that the stability occurs for any initial disturbance.

(ii) Anticyclonic case ($\Omega < 0$) with $\frac{1}{2}W < |2\Omega + W| < W$. The unstable oblique modes are shifted towards spanwise wavevectors ($\frac{1}{2} \leqslant |\cos\theta| \leqslant 1$). The location on spanwise $\boldsymbol{k}$ holds for zero tilting vorticity ($2\Omega + \frac{1}{2}W = 0$) at vanishing D. If $\boldsymbol{k}$ (for the most unstable modes) tends to be aligned with the rotation axis, the disturbances of both vorticity $\hat{\boldsymbol{\omega}}$ and velocity $\hat{\boldsymbol{u}}$ tend to be located in the plane of the mean strain, and the amplification is particularly important.

(iii) Anticyclonic case ($\Omega < 0$) or cyclonic case ($\Omega > 0$) with $|2\Omega + W| > W$. The unstable oblique modes are shifted towards transverse wavevectors ($0 \leqslant \cos\theta \leqslant \frac{1}{2}$). For high rotation rates (cyclonic and anticyclonic), the unstable domain is close to the transverse wave-plane ($\boldsymbol{k} \perp \boldsymbol{\Omega}$) and the amplification is strongly reduced. Note that the instability band with R less than -1 has very much smaller growth rates than that with positive R.

Except for the results at zero absolute vorticity, which are valid for arbitrary strain rates D, the above discussion is suggested by an analysis at weak D. Two ratios $2D/W$ are chosen for the numerical study: the first ($2D/W = 0.05$) gives a weak ellipticity and the second ($2D/W = 0.8$) gives an aspect ratio of the eddy equal to 3. The latter value corresponds to the maximum amplification rate, as shown by Waleffe (1989).

In accordance with a Floquet's analysis, the stability problem amounts to determining the maximum eigenvalue of $\boldsymbol{g}$ after a period $T = 2\pi/\Omega_0$, or $s = \exp[\alpha D T]$. The instability occurs for $\alpha > 0$ or $g_{\gamma\gamma}(\boldsymbol{k}/k, T, 0) > 2$, in accordance with $g_{\alpha\beta}(\boldsymbol{k}/k, 0, 0) = \delta_{\alpha\beta}$ and $\det \boldsymbol{g}(\boldsymbol{k}, T, 0) = 1$. Two types of visualization are presented.

The first one (figure 4*a–f*) (plate 1) represent half a sphere of radius unity viewed both in perspective and in a polar stereographic projection (see figure 5), with each point representing a wavevector direction. The surface is coloured according to the value of the non-dimensional Floquet parameter α (blue for the $\alpha = 0$ stable zone, red for the most unstable case $\alpha \sim 1$). The figures indicate that except for very small $2D/W$, the distribution of α is not axisymmetric, but is characterized by two planes of symmetry ($k_1 = 0$ and $k_2 = 0$) where the width of the instability band (in terms of $\cos\theta$) is either largest or smallest. This distribution motivated figures 6 and 7, diagrams with segments whose length is proportional to the width of the instability band (different values of R and fixed values of the ratio $2D/W$, either for $k_1 = 0$ or $k_2 = 0$, are shown). The (diamond) symbol indicates the location of the

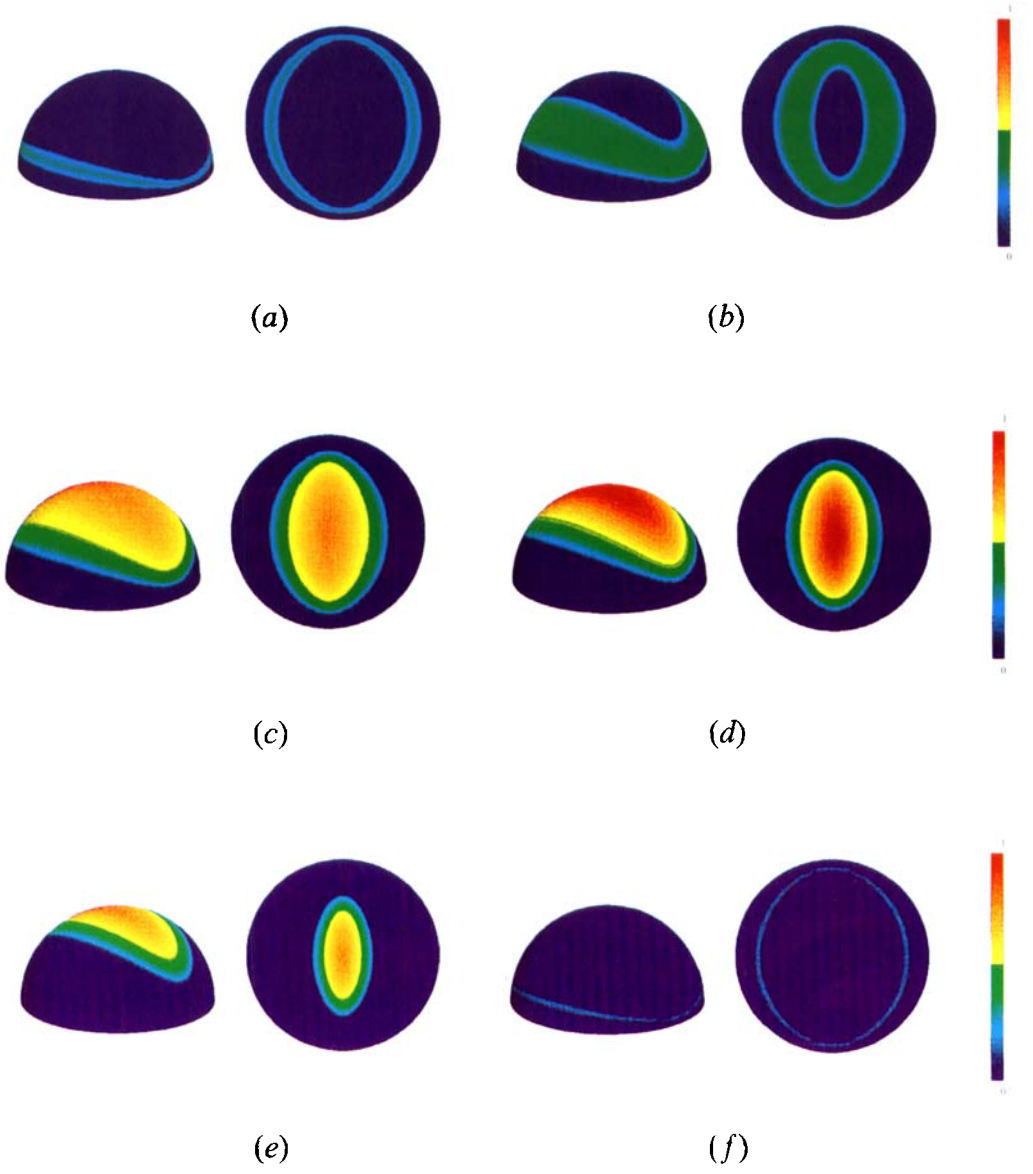

FIGURE 4. Non-dimensional Floquet parameter α: cyclonic background rotation $R = 1$ (*a*); no background rotation $R = 0$ (*b*); anticyclonic background rotation $R = -\frac{1}{4}$ (*c*), $R = -\frac{1}{2}$ (*d*), $R = -\frac{3}{4}$ (*e*), $R = -3$ (*f*).

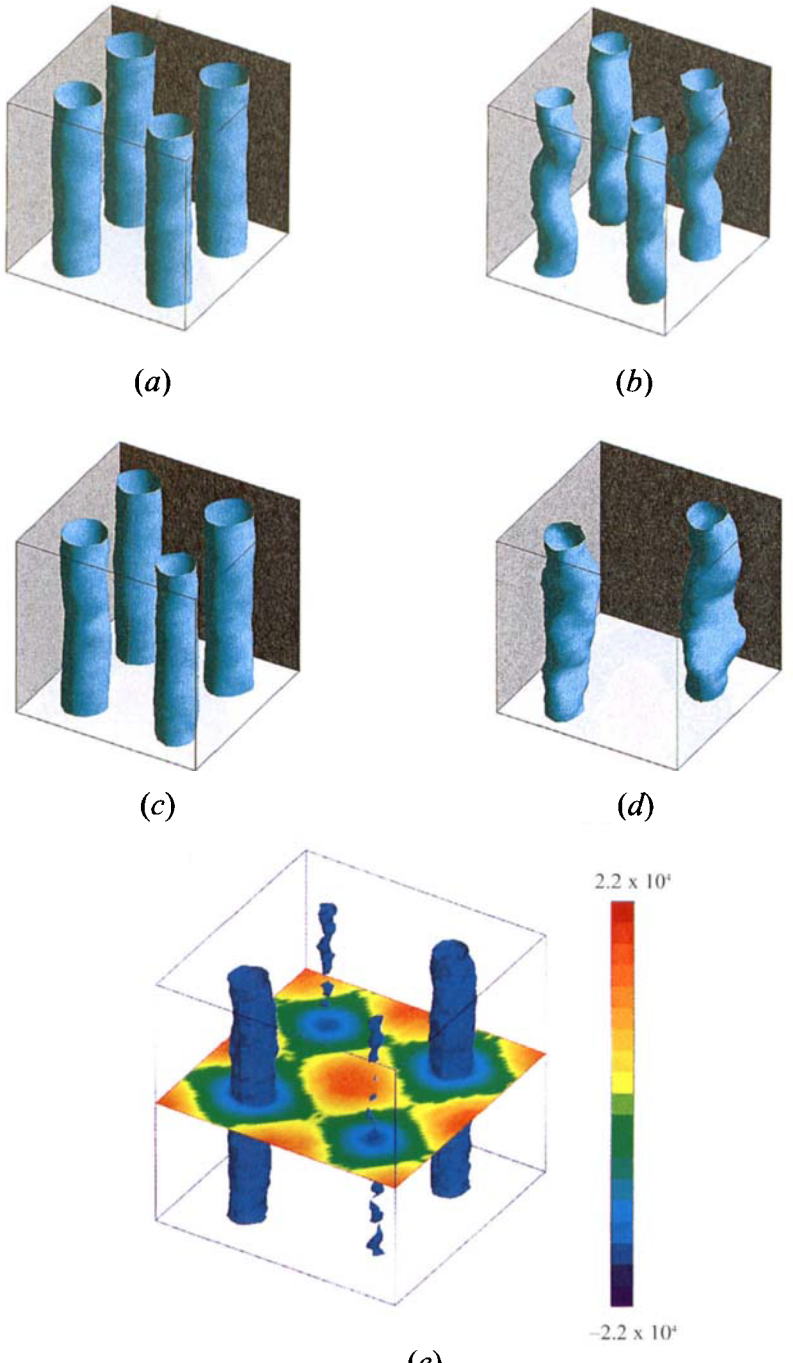

FIGURE 11. Iso-P^{NL} surfaces: initial structure of the turbulent field (*a*), structure obtained after 5 large-eddy turnover times with no rotation (*b*), zero absolute vorticity (*c*) and zero tilting vorticity (*d*) initially in the core of the anticyclonic eddies, zero tilting vorticity using a larger window for sampling iso-surfaces and including a planar cut without threshold (*e*).

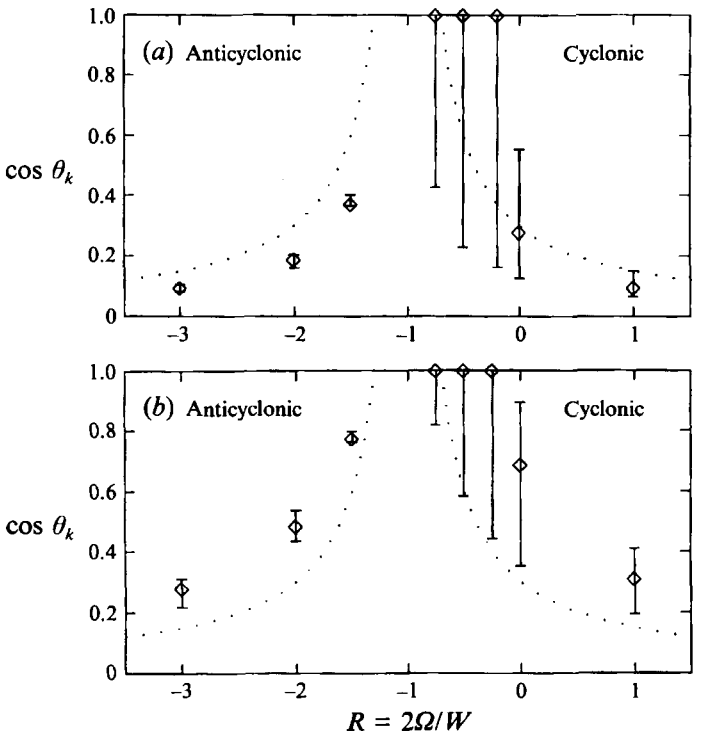

FIGURE 6. Instability bandwidth versus rotation number for elliptical flows within a rotating frame, $2D/W = 0.8$, plane $k_1 = 0$ (*a*) , $k_2 = 0$ (*b*).

maximum α. This second type of visualization was also used by Craik, but only for $k_1 = 0$; it represent an azimuthal cut of the three-dimensional diagrams shown above. The presentation used by Bayly (1986) – without basic rotation – corresponds to a plane rotated, with respect to $k_1 = 0$, by $\pi/4$ ($k_1 + k_2 = 0$) and is thus somewhat less typical. Of course, because of the periodic motion of the wave vector, different azimuthal planar cuts correspond to different initializations of the wavevector, as pointed out by Craik (1989), but visualizations as in figure 4(*a–f*) give additional 'synoptic' information. This latter information is interesting from the point of view of a subsequent RDT calculation, where the contributions from all wavevectors are *simultaneously* taken into account. At weak ellipticity ($2D/W = 0.05$), the instability band is very thin and quasi-axisymmetric. Despite the high resolution of our angular mesh (5101 points equally distributed on half a radius-unity spherical shell) the instability peak is captured only for a few values of R (see figure 7), but the location of the segments on the curve (dotted line) corresponding to (3.10) is recovered. The case of large ellipticity ($2D/W = 0.8$) is illustrated by both three-dimensional and two-dimensional diagrams. In accordance with the discussion following (3.10), figure 4(*b*) shows the reference case without rotation $R = 0$; figure 4(*a*) shows a cyclonic case ($R = 1$) and figure 4(*f*) an anticyclonic case $R = -3$, which represent $|2\Omega + W| > W$ (shift towards equatorial plane); figure 4(*c–e*) represents the most unstable situation with a shift towards the polar zone (the completely stable case $R = -1$ is not given).

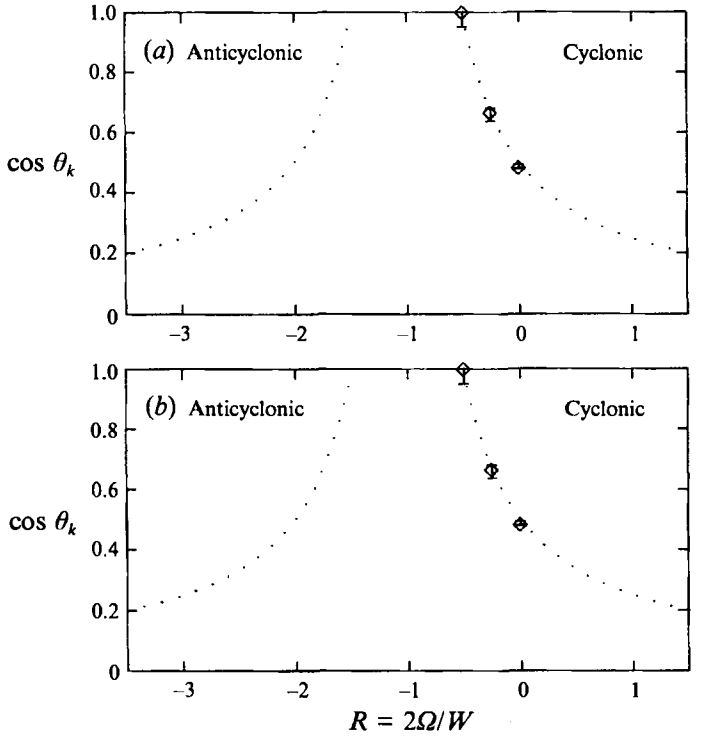

FIGURE 7. Instability bandwidth versus rotation number for elliptical flows within a rotating frame, $2D/W = 0.05$, plane $k_1 = 0$ (a), $k_2 = 0$ (b).

In addition to these stability diagrams, global quantities are shown. Figure 8(a) presents histories for four cases ($R = 1; 0; -\frac{1}{2}; -1$) mentioned above where the final time corresponds to one $2\pi/\Omega_0$ period. The amplification of kinetic energy for the zero-tilting-vorticity case is very striking: the *angular* instability (near $\cos\theta = 1$) is reflected even by the history of an angular-averaged quantity. The case of zero absolute vorticity is found to be stable, whereas an unquestionable instability is captured for the cyclonic ($R = 1$) case. Figure 8(b) shows the damping of the instability for $R = -1$ in the viscous case. The vorticity histories are shown for the same conditions in figure 9. They present the same behaviour for the energy histories and the periodic evolution found for $R = -1$ (zero absolute vorticity) and therefore – since they agree with the exact solution for ω at zero absolute vorticity (see (2.3) and (3.3)) – confirm the accuracy of our numerical method.

4. Numerical simulation of rotating turbulence in the presence of initially two-dimensional Taylor–Green vortices

The initial background field is an array of Taylor–Green vortices. This flow is two-dimensional, space-periodic (in L), and is an exact solution of the N–S equations with a self-similar viscous decay. The streamfunction $\Psi(x_1, x_2)$ is

$$\Psi = \frac{W_0}{2(L/2\pi)^2} \sin 2\pi\frac{x_1}{L} \sin 2\pi\frac{x_2}{L}.$$

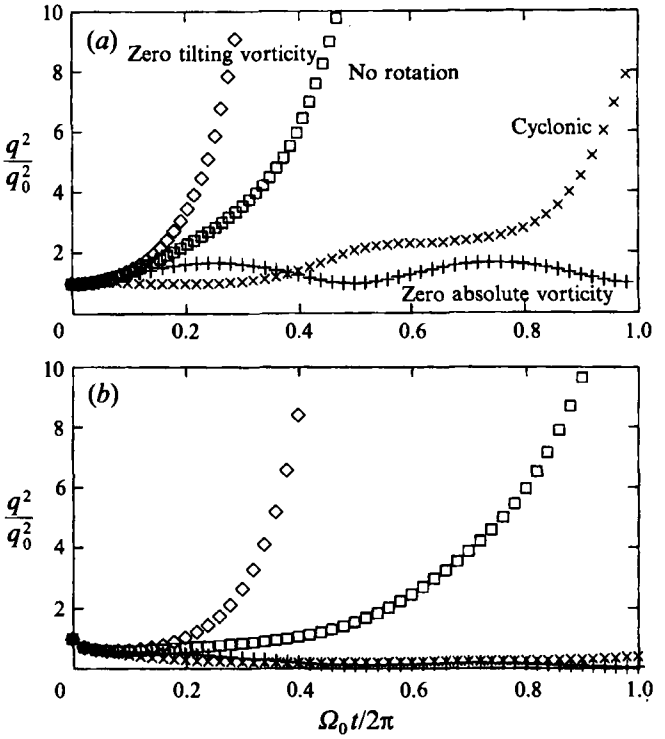

FIGURE 8. Kinetic energy histories for elliptic inviscid case (*a*), viscous case (*b*): ◇, $R = -\frac{1}{2}$; □, $R = 0$; +, $R = -1$; ×, $R = 1$.

It is proportional to the spanwise vorticity, whose maximum value is W_0. From the velocity field

$$U_1 = \frac{\partial \Psi}{\partial x_2}, \quad U_2 = -\frac{\partial \Psi}{\partial x_1},$$

the velocity gradient matrix is recovered

$$\left.\begin{aligned} U_{i,j} &= \begin{pmatrix} D & -\frac{1}{2}W \\ +\frac{1}{2}W & -D \end{pmatrix} \\ \text{with} \quad D(x_1, x_2) &= \tfrac{1}{2} W_0 \cos 2\pi \frac{x_1}{L} \cos 2\pi \frac{x_2}{L}, \quad W(x_1, x_2) = W_0 \sin 2\pi \frac{x_1}{L} \sin 2\pi \frac{x_2}{L}. \end{aligned}\right\} \tag{4.1}$$

Here D and W are the *local* strain rate and *local* vorticity. An 'elementary cell' is shown in figure 10(*a*, *b*) with $(-L/2 < x_1 < L/2, -L/2 < x_2 < L/2)$. The spatial distribution of Ψ (or W) is shown in figure 10(*a*). The four counter-rotating (with respect to each other) eddies are illustrated; their boundaries ($W = 0$) are straight lines, so that four squares are exhibited. Figure 10(*b*) presents the parameter $\sigma^2 = D^2 - (W/2)^2$ (also equal to $-\frac{1}{2}\nabla^2 P$) under the same conditions. The cell consists of diamond-shaped meshes and the straight lines characterize a local pure shear ($\sigma = 0$).

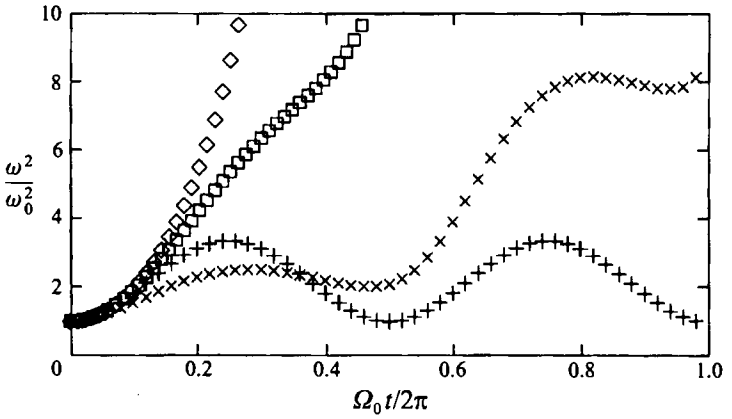

FIGURE 9. Enstrophy histories for elliptic inviscid case: symbols as in figure 8.

The diamond at the centre of the cell is a strain-dominated zone ($\sigma^2 > 0$), while the four surrounding diamonds are vortex-dominated zones (with $\sigma^2 < 0$). If such a flow is set into solid-body rotation, no effect of the Coriolis force is found, in accordance with the geostrophic equilibrium that is valid in a strict two-dimensional limit. Hence, a three-dimensional turbulent field is initially superimposed on the array of Taylor–Green vortices, according to standard procedures for generating initially three-dimensional isotropic homogeneous turbulence. In order to have a fully nonlinear approach, the kinetic energy of the three-dimensional turbulent field is about 15% of the energy of the Taylor–Green vortices. The large-eddy simulation was carried out using a conventional pseudo-spectral code (in agreement with the periodic boundary conditions) with moderate resolution (32^3). A 'Kraichnan-type' (Kraichnan 1976) subgrid-scale model is chosen, with the constants given by Chollet & Lesieur (1981). This procedure yields correct simulations at large Reynolds number ($Re \sim 10^5$ based on the diameter of one of the large vortices) if we only consider the results for the largest scales and during early times, before internal scales become too large for the computational domain.

Results are shown in figure 11 (*a–e*) (plate 2). Iso-vorticity surfaces are not very informative since it has been shown that the structure of the large Taylor–Green vortices is completely masked by the small-scale intense vorticity of the three-dimensional 'turbulent' field. This again illustrates strongly nonlinear features. Thus, eddy structures are visualized by iso-pressure surfaces, in accordance with modern approaches to topological flow structure (Chong *et al.* 1990). More precisely, nonlinear pressure terms are considered, in accordance with the general Poisson equation

$$\nabla^2 P = 2\Omega_i W_i - U_{i,j} U_{j,i} \quad \text{or} \quad \nabla^2 P = \nabla^2 P^L + \nabla^2 P^{NL}, \tag{4.2}$$

where capital letters characterize the total field (without splitting into basic and fluctuating fields). If the total pressure field $P = P^L + P^{NL}$ is considered, the structure of the four eddies at the initial time is not recovered if the rotation rate is chosen to coincide with half the core vorticity (angular velocity) of a Taylor–Green vortex. This result reflects only the fact that the total pressure field is sensitive to the absolute vorticity (according to (2.8)). It does not mean that the dynamics of vortex structures are governed by absolute vorticity (as is, for example, assumed by Lesieur 1990). Accordingly, only the term P^{NL} in (4.2) has been used in subsequent

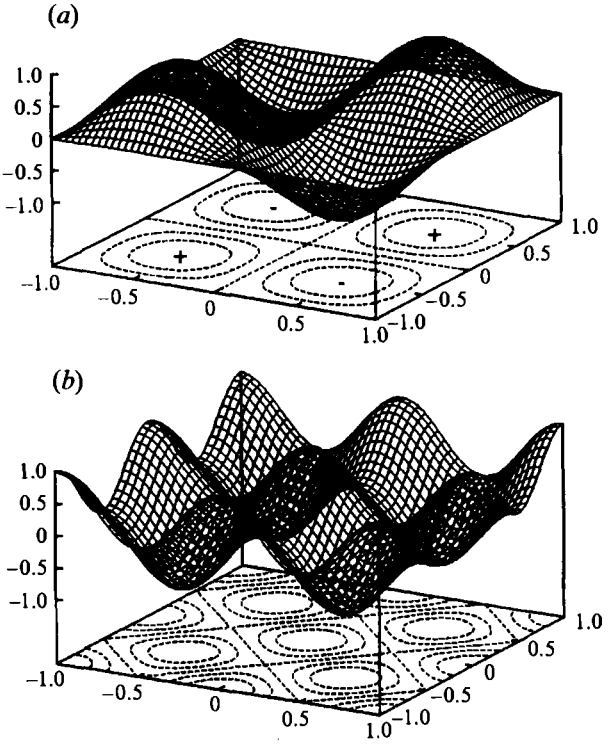

FIGURE 10. Spatial distribution of the streamfunction or vorticity (*a*), and σ^2 or $-\frac{1}{2}\nabla^2 P$ (*b*), within an elementary cell.

visualizations. The initial structure of the turbulent field is recovered using this method, as shown in figure 11 (*a*), and is the same for rotating or non-rotating cases. Three cases have been selected to show the eddy structures obtained after a few (five) turnover times ($4\pi/W_0$). For reference, the case without rotation is shown in figure 11 (*b*). Oscillations in the spanwise direction are exhibited, implying that a destabilization (three-dimensionalization) of the initially organized field, through nonlinear interactions, is in progress. The case where the rotation rate exactly balances the angular velocity in the core of the anticyclonic Taylor–Green vortices is shown in figure 11 (*c*) (zero absolute vorticity). No important destabilization is found, especially with respect to the non-rotating case. Results obtained when the rotation rate balances half the angular velocity (zero tilting vorticity) are shown in figure 11 (*d*). The two anticyclonic eddies no longer appear in the figure, so that a complete breakdown is suspected. The two cyclonic eddies are still present, but their structure is somewhat 'scrambled'. At later time, a merging of these cyclonic eddies is observed. Nevertheless, a refined analysis of the case shown in figure 11 (*d*), using several values of the visualization parameters, has shown that the iso-pressure surface completely disappears in the core of the anticyclonic eddies when the threshold value for sampling the iso-pressure surface is too high: only contributions with intense negative ΔP (pressure differential with respect to a neutral reference value) are shown in figure 11 (*d*). Using a less drastic window (top and bottom threshold values), the anticyclonic eddies are still present, but attenuated, as shown in figure 11 (*e*). In addition, a planar cut has been visualized: this plane is coloured with respect to

the iso-pressure colour-scale and shows that the initial diamond-shaped structure is preserved, with red convergence zones ($\nabla^2 P < 0$ and $\Delta P > 0$) and blue vortex zones ($\nabla^2 P > 0$ and $\Delta P < 0$), in spite of the strong attenuation of the negative pressure differential in the core of the large anticyclonic vortices.

This simple numerical experiment warrants further investigation, but preliminary results are consistent with the criterion of zero tilting vorticity for maximum destabilization, even for a complex flow (inhomogeneous) including nonlinearities. Zero absolute vorticity is also shown to be associated with stabilizing effects.

5. Revisiting effects of rotation on initially unstructured turbulence

It is interesting to discuss to what extent the stability analyses presented above are relevant for a better physical understanding of fully developed initially unstructured turbulent flows subjected to rotation. The recent experiment by Jacquin (1987), Jacquin *et al.* (1990) has exhibited two transitional Rossby numbers Ro^1 and Ro^2, that delimit three regimes for the rotating homogeneous turbulent flow. The Rossby number is the inverse of the rotation number, or $Ro = W/2\Omega$, but its physical relevance depends on the choice of the *effective* W. Jacquin proposed $W = w/L_{33,3}$ as the best indicator, in the light of a rational interpretation of his experimental results, where w is a r.m.s. (along the rotation axis spanwise) velocity component, and $L_{33,3}$ is the integral lengthscale associated with spanwise separation (along the axis of rotation) and spanwise velocity components. A macro Rossby number Ro^L is defined following this choice. A micro Rossby number Ro^λ can be defined by choosing for W the r.m.s. enstrophy ω, so that the Taylor microscale λ is used instead (according to $\omega \sim w/\lambda$). The latter preliminary definitions being born in mind, the three regimes mentioned above are as follows:

(i) For $Ro^L > Ro^1$, the rotation is too small, and the turbulent flow is unaffected by the Coriolis force.

(ii) For $Ro^2 < Ro^L < Ro^1$ (intermediate range), rotation affects the initial isotropic structure of the flow. Integral lengthscales strongly depart from isotropic relationships. For a continuously decreasing Rossby number, $Ro^L = Ro^1$ is shown to characterize a sudden transition, at which the anisotropy (reflected primarily by the lengthscales) is triggered.

(iii) For $Ro^L < Ro^2$, the anisotropy trends are no longer forced, the dissipation rate is strongly reduced.

The values $Ro^1 = 1$ and $Ro^2 = 0.2$ were found in the experimental approach. These results were predicted with an excellent agreement by a nonlinear theory of EDQNM (eddy-damped quasi-normal Markovian theory) type (Cambon 1982; Jacquin 1987; Cambon & Jacquin 1989). This statistical theory can be seen as a stochastic model for nonlinear interactions modified by inertial waves. Apart from the precise finding of the first transition ($Ro^L \sim 1$), discussed further below, DNS up to 256^3 (Mansour, Cambon & Speziale 1991*a*, *b*) have confirmed the existence of this intermediate range of Rossby numbers and have brought to light the second transition ($Ro^L = Ro^2$). In addition, EDQNM, DNS and experimental results have suggested a physical interpretation: $Ro^L = Ro^2$ corresponds to a *micro*–Rossby number close to unity; in this case, the rotation is dominant with respect to the local vorticity of all scales up to the dissipation range. For $Ro^L < Ro^2$ (or $Ro^\lambda < 1$), the nonlinear transfer terms are essentially shut off, due to the angular dispersivity of interacting inertial waves, so that a pure viscous decay is obtained. This interpretation has nothing to do with the Taylor–Proudman theorem, used (at vanishing Rossby numbers) to avoid the problem

of transition from three-dimensional to two-dimensional turbulence. Studies of linear and weakly nonlinear regimes including inertial waves and the geostrophic mode, a relevant regime at small Rossby numbers, have shown that the Taylor–Proudman theorem cannot predict the two-dimensionalization in homogeneous turbulence. As recalled by Mansour *et al.* (1991*a*), among other authors, the time derivative of the fluctuating vorticity remains of the same order of magnitude as Ω, so that a necessary condition for the Taylor–Proudman theorem to be valid is not fulfilled. This theorem is relevant only in the presence of geometric constraints (thin layers) or boundary effects, or external forcing with a *given* (large with respect to Ω^{-1}) timescale. In the same way, the anisotropic trends shown at intermediate Rossby numbers are close to a weak Taylor–Proudman reorganization, but they are mediated by nonlinear interactions. If the homogeneous turbulent field initially includes large-scale quasi-two-dimensional turbulence, as numerically studied by Dang & Roy (1985), these two-dimensional vortex structures are found to be stabilized at small Rossby number, but this stabilization is clearly due to the suppression of the nonlinear transfer terms. These transfer terms are less reduced at higher Rossby number ($Ro^{\lambda} > 1$) and their anisotropic structure (confinement in particular angular-dependent zones in spectral space) underlies anisotropic trends observed in physical space at intermediate Rossby numbers (see also Waleffe 1993). Such explanations are consistent within all the works quoted in this section.

The idea of a transition associated with a stability criterion seems at first glance to be supported by the numerical results of Bartello, Métais & Lesieur (1994), but the latter authors consider a *micro*–Rossby number ($Ro^{\lambda} \sim 1$) and invoke the heuristic criterion of Lesieur (1990).

On the other hand, it is more convincingly suggested that the first transition $Ro^{L} \sim 1$ identified by Jacquin *et al.* (1990), could involve the instability condition at zero tilting vorticity. It is admitted that $W \sim w/L$ characterizes the vorticity in the core of large eddies, whereas $W = \omega \sim w/\lambda$ characterizes the vorticity of dissipative structures inserted between the largest eddies. Accordingly, the magnitude of the intermediate range of Rossby numbers strongly depends on the ratio L/λ and therefore, on the Reynolds number. A clear separation between the two transitions can be obtained only for sufficiently large Reynolds numbers, as already stressed by Jacquin *et al.* (1990). Hence new DNS (or LES) are needed to fulfil these requirements (in terms of both Reynolds and Rossby numbers), thus allowing the first transition to be captured and interpreted.

6. Conclusions

The stability of two-dimensional organized structures imbedded in three-dimensional turbulence and subjected to rotation has been studied in this paper. The conventional Bradshaw–Richardson analogy and the review of the basic equations for both velocity and vorticity have suggested that a maximum destabilization occurred for zero tilting vorticity ($\frac{1}{2}W + 2\Omega = 0$ or $R = -\frac{1}{2}$), whereas the case of zero absolute vorticity ($W + 2\Omega = 0$ or $R = -1$) is quite a stabilizing one. Exact stability analysis and large-eddy simulation of canonic flows were performed in order to check the applicability of such conjectures. First the case of planar mean flows which have quadratic streamfunctions and arbitrary rates of strain and vorticity is considered. For all situations (hyperbolic, linear and elliptical streamlines) the stability analysis, possibly extended towards a statistical RDT approach, confirms that the zero-tilting-vorticity condition gives the maximum destabilization. In addition, the case of zero

absolute vorticity is always found to be more stabilizing than the case without rotation. The difference between the two cases ($R = 0$ and $R = -1$) is particularly striking for pure shear and the elliptical eddy in a rotating frame. The latter fact is not taken into account by the Bradshaw–Richardson criterion, since the two cases correspond to the same (zero) value of B, according to a so-called neutral case. The most promising consequences of this analysis are expected for the case of the rotating elliptical eddy. It is hoped that the latter stability analysis could be applied to the study of the stability of rotating mixing layers, where large oval vortices (with an aspect ratio of 2 or 3) are present. In this sense, our analysis conflicts with a heuristic argument presented by Lesieur (1990) in which maximum destabilization is assumed for zero-absolute-vorticity, whereas the Proudman–Taylor theorem is advocated for explaining the stabilization at high rotation rate. Our analysis shows, in agreement with the similar study by Craik (1989), that the zero-absolute-vorticity case corresponds to unconditional stabilization. Weak destabilization could occur at high rotation rates, but viscous effects are sufficient to eventually damp unstable modes.

In order to examine a nonlinear approach to inhomogeneous turbulence, an array of Taylor–Green vortices is finally considered. The large-scale velocity gradient matrix of this flow has locally the same structure as the *quadratic* flow previously considered, but its parameters are continuously varying in space, so that strain-dominated zones are inserted between vortex-dominated zones. In contrast to the case of a rotating mixing layer, the initial large eddies are counter-rotating with respect to each other. The LES confirm the attenuation of the anticyclonic eddies for zero tilting vorticity, whereas the case of initially zero absolute vorticity in the core of the anticyclonic eddies is shown to be stabilizing. Finally, most of our results suggest that the maximum destabilization of vortex structures could be obtained from the equality

$$\alpha_D (W + 2\Omega) = \tfrac{1}{2} W, \tag{6.1}$$

where W is the spanwise vorticity and α_D depends on the additional straining process and/or on the wavevector of the disturbance (see for example (3.10)). The value $\alpha_D = 1$, for which the zero-tilting-vorticity case is recovered, seems to be a good approximation, valid for diverse situations investigated in this paper. Consistent arguments are given at the end of the paper by Yanase *et al.* (1992) who compared the orientation of the vortex tubes with the orientation of the principal axes of the additional strain matrix.

The authors are indebted to Fabian Waleffe, Julian Scott and Gary Coleman for helpful discussions and assistance. A preliminary version of this paper appeared in a special volume dedicated to Professor Ambarish Ghosh on his sixtieth birthday (*Some Applied Problems in Fluid Mechanics*, edited by H.P. Mazumdar from the Indian Statistical Institute, Calcutta).

Appendix A. The criteria of Bradshaw and Rayleigh

Consider a two-dimensional velocity field $(0, V_\theta, 0)$ in a cylindrical coordinate system (r, θ, z) representing, for instance, a rectilinear vortex or swirl. Such flows possess an absolute vorticity given by

$$\Omega_a = \frac{1}{r} \frac{\partial r V_\theta}{\partial r}.$$

This vorticity can be split into the relative vorticity,

$$W = r\frac{\partial V_\theta / r}{\partial r}$$

and the entrainment vorticity

$$2\Omega = 2\frac{V_\theta}{r}.$$

Rayleigh's stability criterion states that the flow is stable with respect to axisymmetric perturbations if Ω_a is positive, that is if its angular momentum (or circulation) rV_θ increases monotonically. In its classical form, Rayleigh's criterion reads

$$\frac{1}{r^3}\frac{\partial (rV_\theta)^2}{\partial r} > 0$$

for stability. Introducing Ω and W one finds that

$$2\Omega\,(2\Omega + W) > 0\,.$$

Division by W^2 leads to the Bradshaw (or Bradshaw–Richardson) criterion,

$$B = R(R+1) > 0$$

with $R = 2\Omega/W$.

Using this decomposition, an analogy can be drawn between two-dimensional vortex or swirl flows and plane rotating shear flows (the shear rate of the cylindrical flow being $-W$). For instance, in a stable line vortex (e.g. a Lamb vortex), R and B go to infinity when $r \to 0$ (solid-body rotation); outside, when $r \to \infty$, one has $R \to -1$ and $B \to 0$ (potential flow). The analogy with rotating shear is thus helpful in explaining the difficulties one encounters in correctly modelling the turbulent stresses in this flow when the 'Richardson number' B spans the whole range $0 \leqslant B \leqslant \infty$ (Jacquin *et al.* 1992).

Finally, let us note that if maximum destabilization in a rotating shear flow occurred for zero absolute vorticity (that is for $B = 0$), as suggested by Lesieur (1990), this would lead to the unsatisfactory conclusion that the peripheral flow of a line vortex (its potential part) is unstable.

Appendix B. Stability analysis for non-homogeneous shear flows

The background shear flow in the rotating frame is given by

$$U_i = U(x_2)\,\delta_{i1}.$$

Starting from (2.1), (2.5*b*), (2.8*a*) and (2.8*b*), a system of two coupled equations for $\omega = \omega_2$ and $\eta = \nabla^2 u_2$ is easily found:

$$\left(\frac{\partial}{\partial t} + U\frac{\partial}{\partial x_1}\right)\omega + \frac{\partial u_2}{\partial x_3}\left(\frac{\mathrm{d}U}{\mathrm{d}x_2} - 2\Omega\right) = 0, \tag{B 1a}$$

$$\left(\frac{\partial}{\partial t} + U\frac{\partial}{\partial x_1}\right)\eta - \frac{\mathrm{d}^2 U}{\mathrm{d}x_2^2}\frac{\partial u_2}{\partial x_1} + 2\Omega\frac{\partial \omega}{\partial x_3} = 0. \tag{B 1b}$$

If two-dimensional disturbances are considered,

$$\omega = a(x_2, k_1)\,\exp[\mathrm{i}(k_1 x_1 - C(k_1)t)], \tag{B 2}$$

the rotation Ω has no effect and the classical Kelvin–Helmholtz instabilities are recovered, with a maximum amplification for

$$\frac{\mathrm{d}^2 U}{\mathrm{d}x_2^2} = 0.$$

For disturbances with a spanwise variability (which are sensitive to Ω), wave-like form (B 2) is not convenient; a form without space and time separation must be accounted for:

$$\omega = a(x_2, k_1, k_3, t)\exp[\mathrm{i}(k_1 x_1 + k_3 x_3)]. \tag{B 3}$$

This has been shown by Waleffe (1990), who used (B 3) for studying the emergence and the stability of streaky structures in the non-rotating case ($\Omega = 0$).

Note that the presence of streaks along the streamwise (x_1) direction and alternated along the spanwise (x_3) direction leads to the enhancing of the vertical vorticity ω. This effect seems to be completely deleted in the case of zero absolute vorticity ($\mathrm{d}U/\mathrm{d}x_2 - 2\Omega = 0$) as shown by (B 1).

Regarding η, it is possible to compare the wave-like form and the exact form used in § 3. From $\hat{\eta} = 0$, valid in the case of infinite pure constant shear without rotation,

$$\eta = \hat{\eta}(K_1, K_2, K_3)\exp[\mathrm{i}\boldsymbol{K}\cdot\boldsymbol{X}]$$

is derived. It can also be written

$$\eta = \hat{\eta}(K_1, K_2, K_3)\exp[\mathrm{i}(\boldsymbol{K}\cdot\boldsymbol{x} - U_1 K_1 t)]$$

according to the definition of moving coordinates

$$X_1 = x_1 - x_2 St = x_1 - U_1 t; \quad X_2 = x_2; \quad X_3 = x_3.$$

The wave-like form of the disturbance is recovered, but only for this particular case (no rotation, constant shear, *for η and not ω*).

REFERENCES

Andersson, H. I. & Kristoffersen, R. 1992 Vizualisations and statistics of simulated turbulence in a rotating channel. *Communication in Euromech 288, Ecole Centrale de Lyon* (see Cambon 1994).

Bardina, J., Ferziger, J. M. & Reynolds, W. C. 1983 *Technical Rep.* TF-19, Stanford University.

Bartello, P., Métais, O. & Lesieur, M. 1994 Coherent structures in rotating three-dimensional turbulence. *J. Fluid Mech.* **273**, 1–29.

Batchelor, G. K. & Proudman, I. 1954 The effect of rapid distortion on a fluid in turbulent motion *Q. J. Mech. Appl. Maths*, **7**, 83–103.

Bayly, B. J. 1986 Three-dimensional instability of elliptical flow. *Phys. Rev. Lett.* **57**, 2160–2171.

Benoit, J. P. 1992 Etude expérimentale et théorique d'une turbulence homogène soumise à des effets couplés de rotation et déformation plane. Thèse de doctorat, Ecole Centrale de Lyon.

Bertoglio, J. P. 1982 Turbulent shear flow within a rotating frame. *AIAA J.* **20**, 1175.

Bidokhti, A. A. & Tritton, D. J. 1992 The structure of a turbulent free shear layer in a rotating fluid. *J. Fluid Mech.* **241**, 469–502.

Bradshaw, P. 1969 The analogy between streamline curvature and buoyancy in turbulent shear flow. *J. Fluid Mech.* **36**, 177–191.

Cambon, C. 1982 Etude spectrale d'un champ turbulent incompressible soumis à des effets couplés de déformation et de rotation imposés extérieurement. Thèse de doctorat d'état, Université Claude Bernard–Lyon I.

CAMBON, C. 1990 Contribution to single and double point modelling of homogeneous turbulence. *Annual Research Briefs*. Center for Turbulence Research, Stanford.

CAMBON, C. 1994 Turbulent flows undergoing distortion and rotation: A report on EUROMECH 288. *Fluid Dyn. Res. J.*, **13** (6), 281–298 (referred to herein as *E288*).

CAMBON, C., COLEMAN, G. N. & MANSOUR, N. N. 1993 Rapid distortion analysis and direct simulation of compressible homogeneous turbulence at finite Mach number. *J. Fluid Mech.* **251**, 641–665.

CAMBON, C. & JACQUIN, L. 1989 Spectral approach to non-isotropic turbulence subjected to rotation. *J. Fluid Mech.* **202**, 295–317.

CAMBON, C., TEISSÈDRE C. & JEANDEL, D. 1985 Etude d'éffets couplés de déformation et de rotation sur une turbulence homogène. *J. Méc. Théo. Appl.* **4**, 629–657 (referred to herein as CTJ).

CHOLLET, J. P. & LESIEUR, M. 1981 Parametrization of small scales of three-dimensional isotropic turbulence utilizing spectral closures. *J. Atmos. Sci.* **38**, 2747–2757.

CHONG, M. S., PERRY, A. E. & CANTWELL, B. J. 1990 A general classification of three-dimensional flow fields. *Phys. Fluids* A **2**, 765–777.

CRAIK, A. D. D. 1989 The stability of unbounded two- and three-dimensional flows subject to body forces: some exact solutions. *J. Fluid Mech.* **198**, 275–292.

CRAIK, A. D. D. & CRIMINALE, W. O. 1986 Evolution of wavelike disturbances in shear flows: a class of exact solutions of the Navier–Stokes equations. *Proc. R. Soc. Lond.* A 406, 13–26.

CRAYA, A. 1958 Contribution à l'analyse de la turbulence associée à des vitesses moyennes. *P.S.T. Ministère de l'Air, no* 345.

DANG, K. & ROY, PH. 1985 Direct and large eddy simulations of homogeneous turbulence submitted to solid body rotation. In *Turbulent Shear Flow* 5. Springer.

ERINGEN, A. C. 1967 *Mechanics of Continua*. Wiley.

GENCE, J. N. & MATHIEU, J. 1979 On the application of successive plane strains to grid generated turbulence. *J. Fluid Mech.* **93**, 501–513.

GREENSPAN, H. P. 1968 *The Theory of Rotating Fluids*. Cambridge University Press.

HERRING, J. R. 1974 Approach of axisymmetric turbulence to isotropy. *Phys. Fluids* **17**, 859–872.

JACQUIN, L. 1987 Etude théorique et expérimentale de la turbulence homogène en rotation. Thèse de doctorat d'état, Université Claude Bernard–Lyon I.

JACQUIN, L., LEUCHTER, O., CAMBON, C. & MATHIEU, J. 1990 Homogeneous turbulence in the presence of rotation. *J. Fluid Mech.* **220**, 1–52.

JACQUIN, L., SALHI, A. & BENOIT, J. P. 1992 On the stabilizing effects of rotation on swirling flows. *Communication in Euromech 288, Ecole Centrale de Lyon* (see Cambon 1994).

JOHNSTON, J. P., HALLEEN, R. M. & LEZIUS, D. L. 1972 Effects of spanwise rotation on the structure of two-dimensional fully developed turbulent channel flow. *J. Fluid Mech.* **56**, 533–557.

KRAICHNAN, R.H. 1976 Eddy viscosity in two and three dimensions. *J. Atmos. Sci.* **33**, 1521–1536.

KRISTOFFERSEN, R. & ANDERSSON, H. I. 1993 Direct simulation of low-Reynolds-number turbulent flow in a rotating channel. *J. Fluid Mech.* **256**, 163–197.

LAGNADO, R. R., PHAN-THIEN, N. & LEAL, L. G. 1984 The stability of two-dimensional linear flows. *Phys. Fluids* **27**, 1094–1101.

LANDMAN, M. J. & SAFFMAN, P. G. 1987 The three-dimensional instability of strained vortices in a viscous fluid. *Phys. Fluids* **30**, 2339–2342.

LEE, M. J., KIM, J. & MOIN, P. 1990 Structure of turbulence at high shear rate. *J. Fluid Mech.* **216**, 561–583.

LESIEUR, M. 1990 *Turbulence in Fluids*, Kluwer. 2nd Edn.

LEUCHTER, O., BENOIT, J. P. & CAMBON, C. 1992 Effects of plane strain and rotation on homogeneous turbulence. *European Turbulence Conference* 4, *Delft*.

MALKUS, W. V. R. & WALEFFE, F. 1991 The transition from order to disorder in elliptical flow: a direct path to shear flow turbulence. *Advances in Turbulence* 3 (ed. A.V. Johansson & P.H. Alfredsson) Springer.

MANSOUR, N. N., CAMBON, C. & SPEZIALE C. G. 1991*a* Theoretical and computational study of rotating isotropic turbulence. *Studies in Turbulence* (ed. T.B. Gatski, S. Sarkar & C.G. Speziale). Springer.

MANSOUR, N. N., CAMBON, C. & SPEZIALE C. G. 1991*b* Single point modelling of initially isotropic turbulence under uniform rotation. *Annual Research Briefs*. Center for Turbulence Research, Stanford University.

MÉTAIS, O., YANASE, S., FLORES, C., BARTELLO, P. & LESIEUR, M. 1991 Reorganisation of coherent vortices in shear layers under the action of solid-body rotation. *Turbulent Shear Flows* 8, *Munich.*

MICHARD, M., MATHIEU, J., MOREL, R., ALCARAZ, E. & BERTOGLIO, J.P. 1986 Grid generated turbulence exhibiting a peak in the spectrum. *European Turbulence Conference* 1, *Lyon.*

PEDLEY, T.J. 1969 On the instability of viscous flow in a rapidly rotating pipe. *J. Fluid Mech.* **35**, 97–115.

PIERREHUMBERT, R.T. 1986 Universal short-wave instability of two-dimensional eddies in an inviscid fluid. *Phys. Rev. Lett.* **57**, 2157–2159.

RAYLEIGH, LORD 1916 On the dynamics of revolving fluids. *Proc. R. Soc. Lond.* **93**, 148–154.

SALHI, A. 1992 Homogeneous turbulent shear flow in a rotating frame: linear analysis (R.D.T.). *Communication in Euromech 288, Ecole Centrale de Lyon* (see Cambon 1994).

SPEZIALE, C.G., GATSKI, T.B. & MAC GIOLLA MHUIRIS, N. 1990 A critical comparison of turbulence models for homogeneous shear flows in a rotating frame. *Phys. Fluids* A **2**, 1678–1684.

TOWNSEND, A.A. 1956 The Structure of Turbulent Shear Flow *revised version* 1976 Cambridge University Press.

TRITTON, D.J. 1992 Stabilization and destabilization of turbulent shear flow in a rotating fluid. *J. Fluid Mech.* **241**, 503–523.

WALEFFE, F. 1989 The three-dimensional instability of a strained vortex and its relation to turbulence. PhD thesis, MIT.

WALEFFE, F. 1990 On the origin of the streak spacing in turbulent shear flows. *Annual Research Briefs.* Center for Turbulence Research, Stanford University.

WALEFFE, F. 1992 Elliptical Flow Instabilities. *Communication in Euromech 288, Ecole Centrale de Lyon* (see Cambon 1994).

WALEFFE, F. 1993 Inertial transfer in the helical decomposition, *Phys. Fluids* A **5**, 677–685.

YANASE, S., FLORES, C., MÉTAIS, O. & RILEY, J.J. 1992 Rotating free shear flows I : linear stability analysis. *Phys. Fluids* A **5**, 2725–2737.